Am J Transl Res 2023;15(4):2460-2480
www.ajtr.org /ISSN:1943-8141/AJTR0149664

Original Article

A necroptosis gene signature predicts prostate cancer recurrence, and is linked to somatic mutation, therapeutic landscape, and immune infiltration

Yibing Wang[1*], Xiali Zhang[2*], Lidong Wu[1], Qian Feng[1], Zhiqiang Luo[1], Tao Zeng[3], Jun Luo[4]

[1]Emergency Department, The Second Affiliated Hospital of Nanchang University, Nanchang 330006, Jiangxi, China; [2]Laboratory Animal Center of Medical, Department of Nanchang University, Nanchang 330006, Jiangxi, China; [3]Deparment of Urology, The Second Affiliated Hospital of Nanchang University, Nanchang 330006, Jiangxi, China; [4]Department of Rehabilitation Medicine, The Second Affiliated Hospital of Nanchang University, Nanchang 330006, Jiangxi, China. [*]Equal contributors.

Received February 14, 2023; Accepted March 20, 2023; Epub April 15, 2023; Published April 30, 2023

Abstract: Objective: Necroptosis, a type of programmed necrotic cell death, has been implicated in cancer biology and therapeutics. Improved risk stratification is required for prostate carcinoma in individuals. In view of the importance of necroptosis, this work proposed a necroptosis-based genetic model for recurrence prediction, and clarified its characteristics. Methods: A least absolute shrinkage and selection operator (LASSO) regression analysis was conducted based upon transcriptome data of necroptosis genes with clinical information in the Cancer Genome Atlas (TCGA) prostate carcinoma samples, which were externally verified in the GSE116918 cohort. Somatic mutation was characterized by Maftools method. The drug sensitivity was estimated via OncoPredict algorithm. T-cell inflammation score and tumor mutational burden (TMB) score were computed for inferring immunotherapy response. CIBERSORT was adopted for scoring the infiltration of immune cell compositions. Results: The necroptosis gene model was defined, composed of BCL2, BCL2L11, BNIP3, CASP8, CYLD, HDAC9, IDH2, IPMK, MYC, PLK1, TNF, TNFRSF1A, and TSC1. Considering external verification, this model effectively predicted recurrence-free survival, notably within one year (area under the curve (AUC) = 0.841, 0.706, 0.776, and 0.893 in the discovery, verification, total and external independent sets, respectively). Patients who had a risk score > median value were defined as high risk, while those who had risk score ≤ median value were defined as low risk. Older age, more advanced T, N, M stage, shorter disease-free survival, and more recurred/progressed statuses were found in high-risk patients (all $P<0.05$). Moreover, the signature independently predicted patient recurrence ($P<0.05$). High-risk specimens had more frequent somatic mutation, especially of TP53, BSN, APC, TRANK1, DNAH9, and SALL1 (all $P<0.05$). The heterogeneity in sensitivity to small-molecule compounds was investigated in low- and high-risk patients. Also, high-risk individuals responded better to immunotherapy ($P<0.05$). Conclusion: Altogether, the necroptosis gene signature may effectively predict prostatic carcinoma recurrence and therapeutic responses, but its clinical feasibility must be verified.

Keywords: Prostatic carcinoma, necroptosis, recurrence, somatic mutation, therapeutic response, immune infiltration

Introduction

Prostate carcinoma remains a leading cause of cancer-related death in men [1]. This malignancy differs from other epithelial tumor types, which lacks recognizable histologic subtypes [2]. Nearly all patients have acinar type, but prostatic carcinoma exhibits much inter- and intratumoral heterogeneity and is variable in disease severity [3]. Localized patients can receive surgical resection or radiotherapy. Nonetheless, the recurrence rate following therapy remains high (25%-35%) [4]. In advanced stages, prostatic carcinoma can spread to distinct parts of the body, especially the bones [5]. Androgen deprivation therapy remains the standard therapeutic regimen for recurrent patients, but prostatic carcinoma cells accom-

modate to androgen deprivation and convert into aggressive status [6]. Hence, accurate recurrence prediction is urgently required.

Necroptosis is a regulated necrotic cell death modality, that can be activated in a caspase-driven manner [7]. This death is triggered by RIP1, RIP3, MLKL, etc., and accompanied by the release of damage-associated molecular patterns and cytokines, thus driving the proinflammatory response [8]. Necroptosis exerts crucial physiologic functions in development and tissue homeostasis, and its deregulation results in varieties of pathologic conditions [9]. Recent studies have unveiled the implications of necroptosis in prostatic carcinoma. For instance, PIK1 suppression can results in necroptosis of androgen-insensitive prostatic carcinoma cells [10]. Up-regulated RIP3 attenuates prostatic carcinoma progression through activating RIP3/MLKL signaling and inducing necroptosis [11]. SIRT3/6 accelerates prostatic carcinoma progression through inhibition of the necroptosis-driven innate immune response [12]. Shikonin lowers growth of docetaxel-resistant prostatic carcinoma cells primarily through necroptosis [13]. Necroptosis acts as an alternative pattern of programmed cell death that overcomes apoptosis resistance, and it can drive and improve antitumor immunity in cancer therapeutics [14]. Thus, accumulating evidence has suggested the use of targeting necroptosis as a therapeutic regimen for prostatic carcinoma [14]. Altogether, this study established a necroptosis-based gene signature for prediction of prostatic carcinoma recurrence, that might assist with designing therapeutic intervention.

Materials and methods

Transcriptome profiling acquirement and preprocessing

Transcriptome data of 499 prostatic carcinoma and 52 normal specimens were gathered from the Cancer Genome Atlas (TCGA) database (https://portal.gdc.cancer.gov/). In addition, clinical data were obtained. Utilizing edgeR package [15], normalization of counted data into CPM was implemented. The GSE116918 cohort comprising microarray expression matrix and recurrence-free survival information of 248 prostate carcinoma patients was acquired from the Gene Expression Omnibus (https://www.ncbi.nlm.nih.gov/geo/query/acc.cgi?acc=GSE116918) on the GPL25318 platform, which was adopted as the external verification set [16]. Supplementary Table 1 lists the clinical features of prostatic carcinoma patients in the TCGA and GSE116918 cohorts. Necroptosis genes were collected from previous research, as listed in Supplementary Table 2.

Differential expression analysis

Genes with aberrant expression were selected in prostate carcinoma versus controls by use of edgeR package. The threshold values were set as q-value <0.05 and |log2fold change (FC)| >1.

Functional annotation analysis

The enrichment of aberrantly expressed genes on Gene Ontology (GO) was conducted through Clusterprofiler package [17]. GO terms are composed of biological processes, cellular components, and molecular functions. Additionally, enriched Kyoto Encyclopedia of Genes and Genomes (KEGG) pathways were analyzed. False discovery rate <0.05 was utilized as the cutoff value.

Least absolute shrinkage and selection operator (LASSO) regression analysis

The stratification of TCGA prostatic carcinoma cases into discovery and verification sets was carried out following a ratio of 1:1. Necroptosis genes were incorporated into the LASSO analysis by use of glmnet package [18]. Under the minimum lambda, genes with coefficient ≠0 were chosen for the model construction. With predict.cv.glmnet function, risk score was computed. Patients in each set were stratified into low- or high-risk groups. Kaplan-Meier curves of recurrence-free survival were then plotted with Survival package. The estimation of survival difference was implemented utilizing log-rank test. Prognostic influence was appraised with receiver operator characteristic curve (ROC) utilizing pROC package. The GSE116918 cohort was adopted for proving the replicability of the model. Clinical traits were compared between low- and high-risk patients. Uni- and multivariate-Cox regression analysis was utilized for appraising independence in recurrence prediction.

Gene set enrichment analysis (GSEA)

GSEA analytical approach [19] was utilized for investigating the relevant GO and KEGG pathways of the prognostic signature based upon the reference gene set that was obtained from the Molecular Signature Database [20]. P<0.05 was set as the enrichment criterion.

Analysis of somatic mutations

Somatic variant data (MAF files) of prostatic carcinoma specimens from TCGA were analyzed and visualized by use of Maftools package [21].

Drug sensitivity estimation

Drug sensitivity data of anti-tumor compounds across tumor cell lines were collected from the Drug Sensitivity in Cancer database v2 [22], and were estimated by use of oncoPredict package [23].

Immunotherapeutic response prediction

T-cell inflammation score was computed following the weighted sum of the standardized transcript levels of eighteen genes (CCL5, CD27, CD274, CD276, CD8A, CMKLR1, CXCL9, CXCR6, HLA-DQA1, HLA-DRB1, HLA-E, IDO1, LAG3, NKG7, PDCD1LG2, PSMB10, STAT1, and TIGIT) as described [24]. In addition, Tumor Immune Dysfunction and Exclusion (TIDE) was scored based upon immune escape mechanisms composed of inducing T cell dysfunction in tumors with highly infiltrative cytotoxic T lymphocytes and preventing T cell infiltration in tumors with lowly infiltrative cytotoxic T lymphocytes [25].

Immune infiltration quantification

The infiltration levels of immune cell compositions were scored, and compared between groups by employing CIBERSORT [26] that combined support vector regression with known expression profiles from purified leukocyte subpopulations. Correlations between immune cell compositions were then estimated.

Statistical analysis

All the analyses were achieved through R platform (version 3.6.1). Continuous variables were compared between groups with Wilcoxon test, while chi-square test was utilized for analyzing categorical data. Correlation analysis between variables was conducted utilizing Pearson's or Spearman's test. P<0.05 indicated significance.

Results

Identification of aberrantly expressed necroptosis genes and their biological functions in prostatic carcinoma

In comparison to 52 control tissues, 720 genes presented significant up-regulation in 499 prostatic carcinoma specimens, with 1258 displaying down-regulation under the threshold of q-value <0.05 and |log2FC| >1 (**Figure 1A**, **1B**; Supplementary Tables 3, 4). **Figure 1C** and **Table 1** illustrate the top 20 up- and down-regulated genes, respectively. Among aberrantly expressed genes, there were seven necroptosis genes. The expression of BCL2, CD40, GATA3, ID1, and TLR3 was markedly lower in prostatic carcinoma versus controls, with higher expression of CDKN2A and PLK1 (**Figure 1D**). Biological significance of the aberrantly expressed genes was further probed. It was found that the development processes of the nervous system, organism, tissues, and cells were enriched (**Figure 1E**). The genes were in relation to plasma membrane components and transmembrane transporter activity (**Figure 1F**, **1G**). In addition, a marked enrichment of tumorigenic pathways (calcium signaling pathway, metabolic pathways, neuroactive ligand-receptor interaction, pathways in carcinoma, PI3K-Akt signaling pathway) was found (**Figure 1H**), indicative of the involvement of aberrantly expressed genes in prostatic carcinoma.

Definition of a necroptosis gene signature for prostatic carcinoma recurrence

A few necroptosis genes were linked with prostatic carcinoma survival (**Table 2**). Necroptosis genes were included in the LASSO analysis. In accordance with a ratio of 1:1, we randomly stratified TCGA prostate carcinoma cases into discovery (n = 236) and verification sets (n = 236). As illustrated in **Figure 2A**, the minimum lambda value was 0.0214. Thirteen genes with coefficient ≠0 were selected for generating the LASSO signature (**Figure 2B**). The formula included: risk score = (-0.025232796) * BCL2 + 0.351117088 *

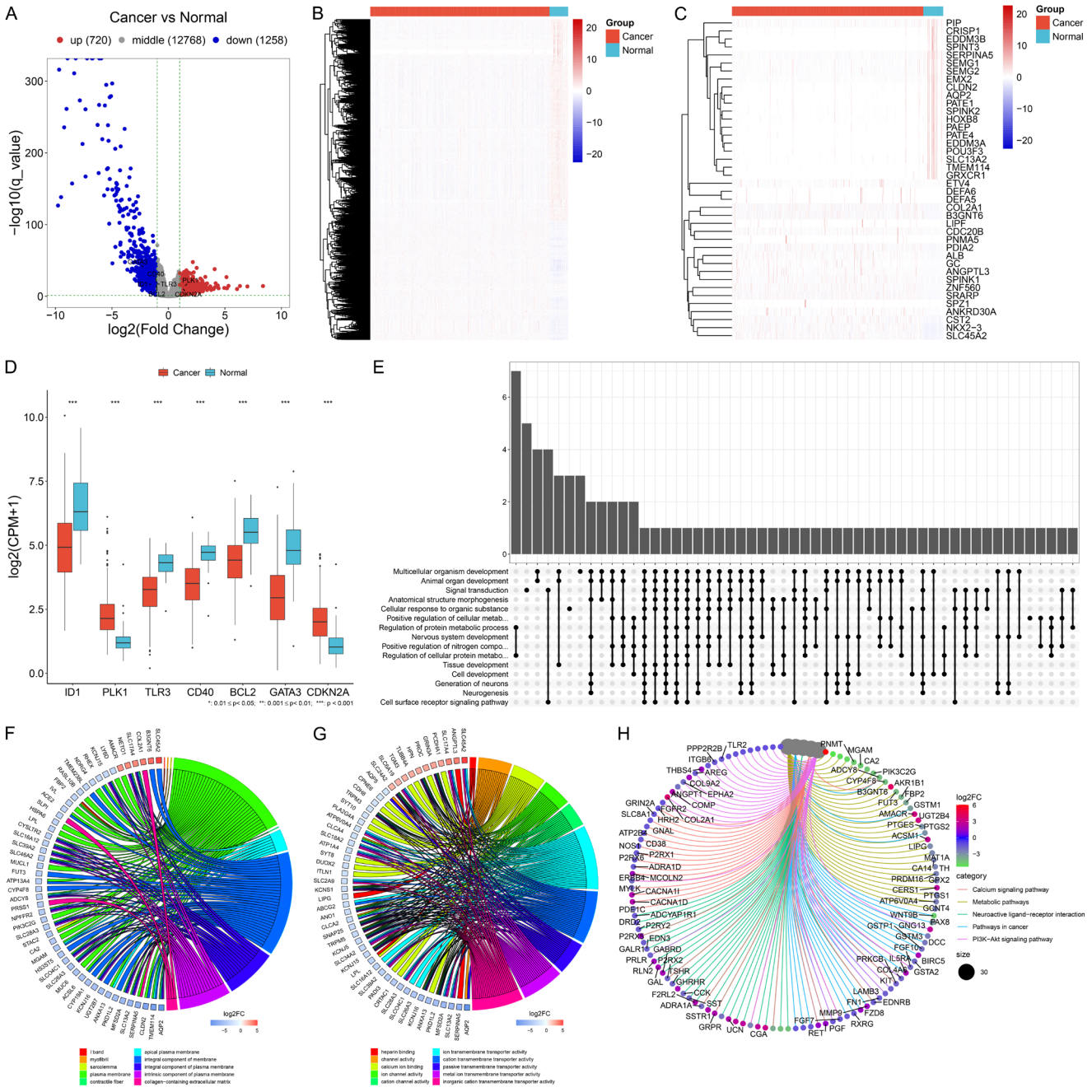
A
Cancer vs Normal
up (720)
middle (12768)
down (1258)
−log10(q_value)
log2(Fold Change)
B
Group
Cancer
Normal
C
Group
Cancer
Normal
PIP
CRISP1
EDDM3B
SPINT3
SERPINA5
SEMG1
SEMG2
EMX2
CLDN2
AQP2
PATE1
SPINK2
HOXB8
PAEP
PATE4
EDDM3A
POU3F3
SLC13A2
TMEM114
GRXCR1
ETV4
DEFA6
DEFA5
COL2A1
B3GNT6
LIPF
CDC20B
PNMA5
PDIA2
ALB
GC
ANGPTL3
SPINK1
ZNF560
SRARP
SPZ1
ANKRD30A
CST2
NKX2−3
SLC45A2
D
Cancer
Normal
log2(CPM+1)
ID1
PLK1
TLR3
CD40
BCL2
GATA3
CDKN2A
E
Multicellular organism development
Animal organ development
Signal transduction
Anatomical structure morphogenesis
Cellular response to organic substance
Positive regulation of cellular metab...
Regulation of protein metabolic process
Nervous system development
Positive regulation of nitrogen compo...
Regulation of cellular protein metabo...
Tissue development
Cell development
Generation of neurons
Neurogenesis
Cell surface receptor signaling pathway
F
log2FC
I band
myofibril
sarcolemma
plasma membrane
contractile fiber
apical plasma membrane
integral component of membrane
integral component of plasma membrane
intrinsic component of plasma membrane
collagen−containing extracellular matrix
G
log2FC
heparin binding
channel activity
calcium ion binding
ion channel activity
cation channel activity
ion transmembrane transporter activity
cation transmembrane transporter activity
passive transmembrane transporter activity
metal ion transmembrane transporter activity
inorganic cation transmembrane transporter activity
H
log2FC
category
Calcium signaling pathway
Metabolic pathways
Neuroactive ligand−receptor interaction
Pathways in cancer
PI3K−Akt signaling pathway
size

Figure 1. Analysis of aberrantly expressed necroptosis genes in prostate carcinoma. A. Volcano diagram of genes with down- (blue) or up-regulation (red) in tumors relative to normal specimens. B. Heatmap illustrating the transcript levels of genes with differential expression in tumors as well as normal tissues. C. The top 20 aberrantly expressed genes. D. The differential expression of necroptosis genes in prostate carcinoma relative to controls. ***P<0.001. E. Upset plot of the biological processes enriched by aberrantly expressed genes. F, G. Circle plots depicting the cellular components and molecular functions. H. Circle plot illustrating the enriched Kyoto Encyclopedia of Genes and Genomes (KEGG) pathways.

Table 1. The top 20 up- and down-regulated genes in prostate carcinoma versus controls

Gene name	log2FC	FC	*p*-value	q-value	Cancer	Normal
DEFA5	8.3716973	331.23178	6.979E-16	5.566E-15	3.491291	-4.880406
DEFA6	6.9898642	127.10388	2.616E-15	1.968E-14	1.7706689	-5.219195
SPZ1	6.3292789	80.408658	6.687E-16	5.348E-15	1.3217759	-5.007503
LIPF	6.0753631	67.432077	1.619E-11	7.903E-11	3.0604344	-3.014929
ANKRD30A	5.3176818	39.882441	3.784E-16	3.114E-15	0.7031271	-4.614555
PNMA5	5.1795183	36.240181	1.473E-12	8.092E-12	1.3770636	-3.802455
SLC45A2	5.1385819	35.226321	5.98E-29	1.676E-27	3.1640713	-1.974511
GC	4.9466627	30.838543	3.721E-13	2.205E-12	0.9274863	-4.019176
SPINK1	4.4416511	21.730525	1.382E-12	7.625E-12	4.8492353	0.4075842
ALB	4.3659141	20.619167	9.664E-17	8.488E-16	3.2312734	-1.134641
PDIA2	4.1799858	18.125964	6.159E-20	7.499E-19	2.1584193	-2.021567
B3GNT6	4.1044857	17.201777	4.861E-14	3.159E-13	3.6464064	-0.458079
NKX2-3	4.0901944	17.032218	2.356E-40	1.412E-38	1.0904984	-2.999696
CDC20B	4.0030346	16.03369	1.366E-11	6.72E-11	1.6551842	-2.34785
ETV4	3.7857493	13.7919	2.508E-10	1.063E-09	5.7510335	1.9652842
COL2A1	3.7756977	13.696142	4.322E-11	2.013E-10	6.2793698	2.5036721
SRARP	3.7330024	13.296756	3.431E-14	2.265E-13	4.3412256	0.6082232
ANGPTL3	3.7013382	13.008099	2.102E-15	1.597E-14	1.4463782	-2.25496
CST2	3.5121391	11.409306	8.107E-13	4.605E-12	4.1760578	0.6639187
ZNF560	3.4570438	10.981809	3.565E-12	1.877E-11	1.0242267	-2.432817
SEMG1	-9.775117	0.0011413	9.63E-130	2.53E-127	4.9716303	14.746747
PAEP	-9.676455	0.0012221	0	0	-2.946652	6.7298034
SEMG2	-9.506544	0.0013748	1.58E-141	4.75E-139	4.2088356	13.71538
AQP2	-9.228468	0.0016671	3.31E-239	2.32E-236	-1.36544	7.8630279
PATE4	-9.02154	0.0019242	4.91E-265	4.26E-262	-2.409024	6.6125164
EDDM3A	-8.933127	0.0020458	0	0	-4.631233	4.3018942
PATE1	-8.526312	0.0027122	1.2E-160	4.8E-158	-0.760548	7.7657641
CRISP1	-8.343793	0.003078	0	0	-3.366585	4.9772082
TMEM114	-8.209693	0.0033778	0	0	-4.320851	3.8888416
CLDN2	-7.843457	0.004354	5.87E-277	6.19E-274	-1.277043	6.5664131
POU3F3	-7.60356	0.0051416	6.05E-216	3.57E-213	-2.827124	4.7764359
SPINK2	-7.341461	0.006166	1.84E-264	1.51E-261	-1.338484	6.0029769
PIP	-7.336798	0.0061859	2.07E-170	9.23E-168	2.4785514	9.8153489
EDDM3B	-7.203837	0.0067831	0	0	-5.211152	1.9926848
SERPINA5	-6.770752	0.009158	0	0	0.9116439	7.6823955
EMX2	-6.718795	0.0094938	0	0	-1.192677	5.5261177
GRXCR1	-6.270399	0.0129545	1.25E-242	9.7E-240	-4.519545	1.7508538
SLC13A2	-6.179377	0.0137982	3.09E-175	1.42E-172	-1.922498	4.2568799
HOXB8	-6.137611	0.0142035	1.36E-270	1.33E-267	-1.873949	4.2636623
SPINT3	-6.121831	0.0143597	0	0	-4.882775	1.239056

Abbreviations: FC, fold change.

Table 2. Univariate-cox regression results on necroptosis genes with prostate carcinoma survival

Gene name	*p*-value	Hazard ratio	Gene name	*p*-value	Hazard ratio
APP	0.08067	0.796726	MAP3K7	0.498697	1.189729
ATRX	0.274205	1.220549	MAPK8	0.339893	1.320766
AXL	0.620242	1.0731	MLKL	0.960695	0.992092
BACH2	0.424107	1.106446	MPG	0.322789	0.729869
BCL2	0.731386	0.958756	MYC	0.032669	1.324089
BCL2L11	0.027728	1.702859	MYCN	0.004015	1.406327
BNIP3	0.318348	1.279589	OTULIN	0.650664	1.143524
BRAF	0.180501	1.322169	PANX1	0.773615	1.07353
CASP8	0.005524	1.84963	PLK1	1.22E-07	1.748096
CD40	0.339445	0.892521	RIPK1	0.122613	0.578499
CDKN2A	0.074661	1.211883	RIPK3	0.240079	1.161234
CFLAR	0.076539	1.743226	RNF31	0.068092	1.469021
CYLD	0.945546	1.016303	SIRT1	0.71625	1.07426
DDX58	0.181327	1.249631	SIRT2	0.906193	0.955716
DIABLO	0.082751	1.720238	SIRT3	0.34527	1.46611
DNMT1	0.003007	2.127006	SLC39A7	0.070014	0.672013
EGFR	0.950282	1.010029	SPATA2	0.760849	1.10469
FADD	0.060086	1.838069	SQSTM1	0.725369	0.9054
FAS	0.799665	0.964879	STAT3	0.154647	0.735785
FASLG	0.949446	1.006383	STUB1	0.571166	1.170124
FLT3	0.191404	1.137832	TARDBP	0.462717	1.525783
GATA3	0.369248	0.936172	TERT	0.372757	1.085314
HAT1	0.93094	0.977497	TLR3	0.963372	1.005153
HDAC9	0.166299	1.124826	TNF	0.540372	0.942796
HSP90AA1	0.814506	1.064178	TNFRSF1A	0.029867	0.528562
HSPA4	0.39442	1.333352	TNFRSF1B	0.710441	1.055717
ID1	0.523155	0.945459	TNFRSF21	0.696004	0.946894
IDH1	0.806092	0.958549	TNFSF10	0.029587	0.736547
IDH2	0.093432	0.656898	TRAF2	0.066766	1.687172
IPMK	0.979017	1.004829	TRIM11	0.077609	1.689431
ITPK1	0.951148	0.984725	TSC1	0.009475	2.159937
KLF9	0.312095	0.823053	USP22	0.304253	1.283789
LEF1	0.368861	1.098597	ZBP1	0.123232	1.149527

BCL2L11 + 0.109512296 * BNIP3 + 0.167468742 * CASP8 + (-0.503197016) * CYLD + 0.211246262 * HDAC9 + (-0.648970979) * IDH2 + (-0.41842532) * IPMK + 0.059209364 * MYC + 0.361009384 * PLK1 + (-0.118982206) * TNF + (-0.05462146) * TNFRSF1A + 0.101005098 * TSC1. Among the selected genes, PLK1, CASP8, TSC1, and BCL2L11 acted as risk factors of recurrence-free survival, with TNFRSF1A as a protective factor (**Figure 2C**). The risk score of each TCGA prostatic carcinoma case was computed (**Figure 2D**). The heterogeneous expression of the selected necroptosis genes was investigated across prostatic carcinoma (**Figure 2E**). In **Figure 2F**, BCL2L11, BNIP3, CASP8, IDH2, IPMK, MYC, PLK1, and TSC1 exhibited up-regulation in tumors relative to control specimens, with down-regulation of BCL2, CYLD, HDAC9, and TNFRSF1A. Patients in the discovery set were classified into low- or high-risk groups. Specifically, patients who had risk score > median value were defined as high risk, while those who had risk score ≤ median value were defined as low risk. In **Figure 2G**, shorter recurrence-free survival was investigated in high-risk individuals. The predictive ability of the signature was also appraised.

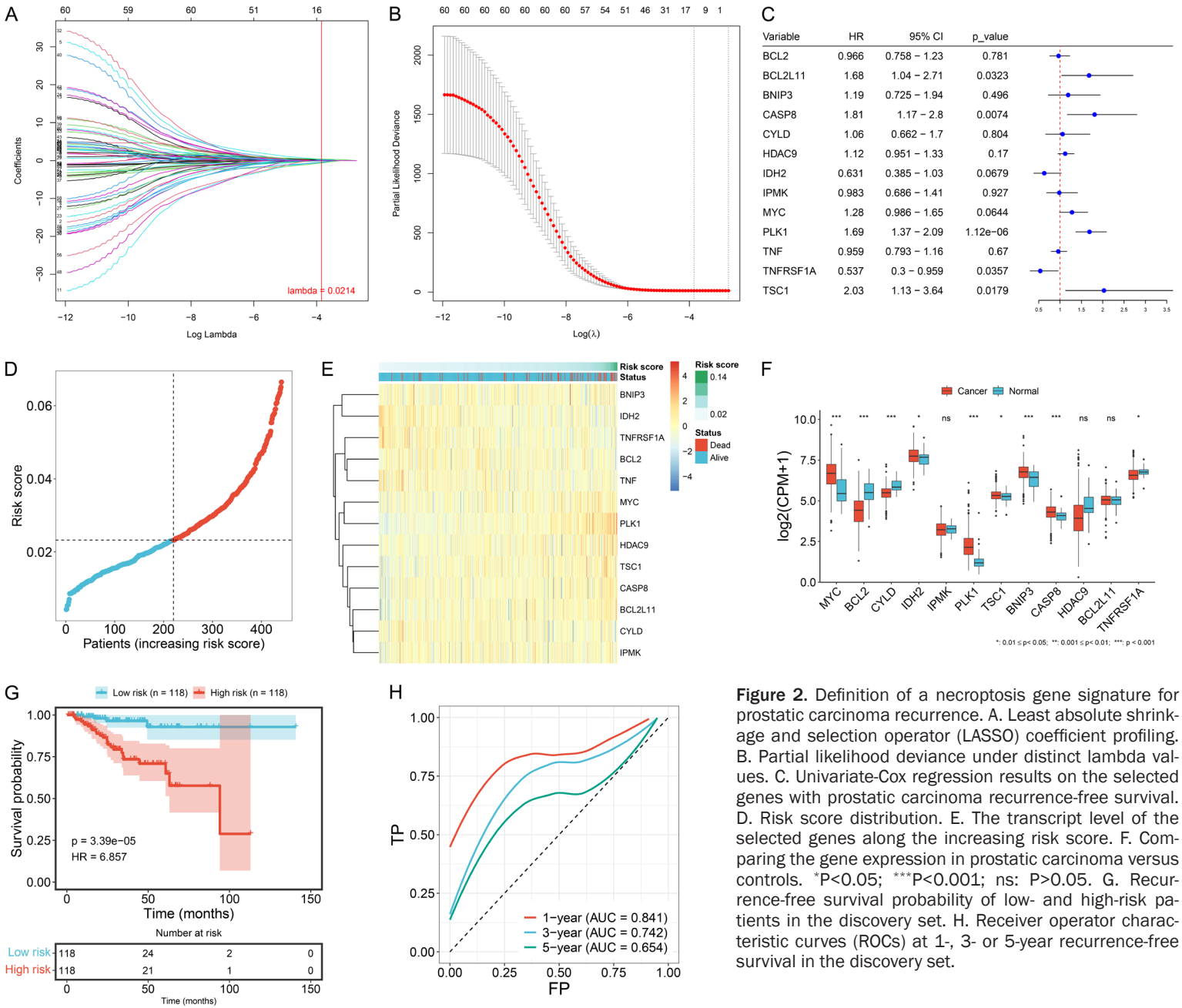

Figure 2. Definition of a necroptosis gene signature for prostatic carcinoma recurrence. A. Least absolute shrinkage and selection operator (LASSO) coefficient profiling. B. Partial likelihood deviance under distinct lambda values. C. Univariate-Cox regression results on the selected genes with prostatic carcinoma recurrence-free survival. D. Risk score distribution. E. The transcript level of the selected genes along the increasing risk score. F. Comparing the gene expression in prostatic carcinoma versus controls. *P<0.05; ***P<0.001; ns: P>0.05. G. Recurrence-free survival probability of low- and high-risk patients in the discovery set. H. Receiver operator characteristic curves (ROCs) at 1-, 3- or 5-year recurrence-free survival in the discovery set.

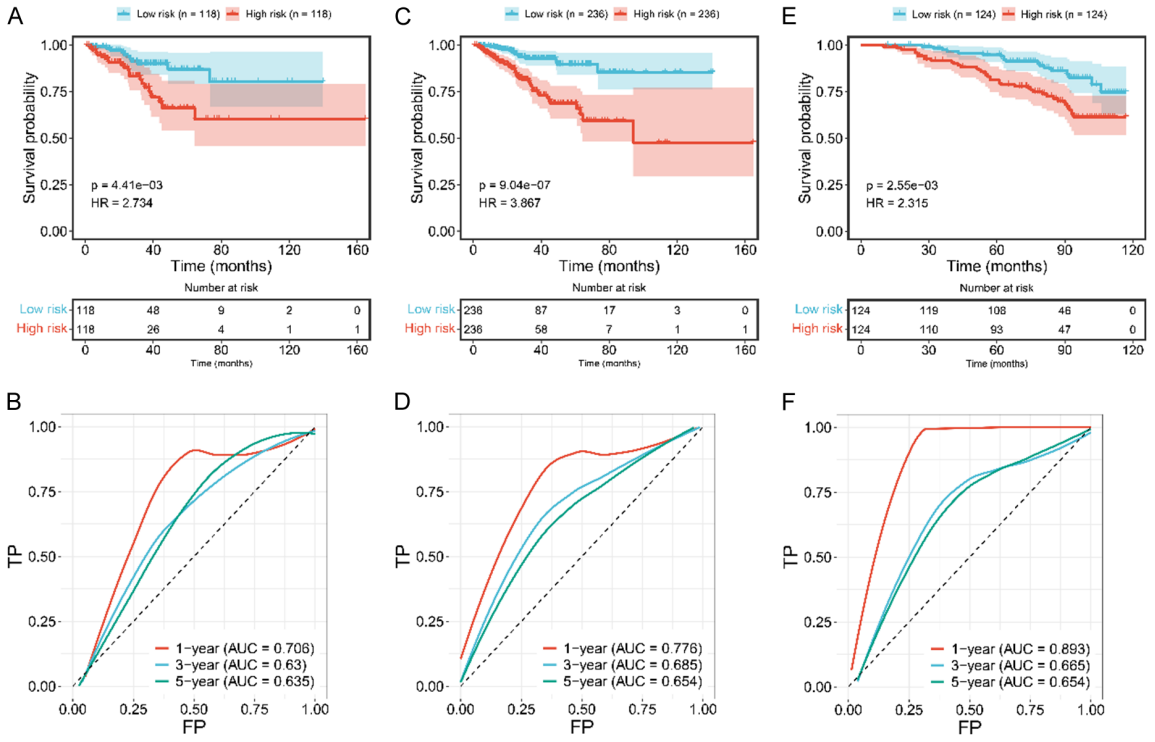

Figure 3. Verification of the necroptosis gene signature for recurrence prediction. A. Recurrence-free survival of low- or high-risk patients in the verification set. B. Receiver operator characteristic curves (ROCs) in the verification set. C. Recurrence-free survival curves of two groups in the total set. D. ROCs in the total set. E. External verification of survival difference between groups in the GSE116918 cohort. F. ROCs in the GSE116918 cohort.

The area under the curve (AUC) values at one-, three- and five-year survival were 0.841, 0.742, and 0.654, respectively (all P<0.0001) (**Figure 2H**). This proved that the signature modestly predicted prostatic carcinoma recurrence.

Verification of the necroptosis gene signature for recurrence prediction

Validation of the prognostic implications of the necroptosis gene signature was then conducted. As expected, high-risk patients had the worse recurrence-free survival relative to those with low risk in the verification set (**Figure 3A**), with >0.60 AUC values (all P<0.0001) (**Figure 3B**). Similar findings were observed in the total set (**Figure 3C**, **3D**). The replicability was proven in the GSE116918 cohort (**Figure 3E**, **3F**). Notably, the necroptosis gene signature possessed the highest accuracy in prediction of recurrence within one year.

Clinical trait relevance of the necroptosis gene signature and its predictive independence

The heterogeneous clinical traits were investigated in low- and high-risk prostatic carcinoma. High-risk cases had an older age (**Figure 4A**). Higher proportions of advanced T, N, and M stages were found in the high-risk group (**Figure 4B-D**). It was also observed that there were more metastatic lymph nodes in high-risk cases (**Figure 4E**). In addition, those with high risk had a shorter disease-free survival (DFS) as well as higher ratio of recurred/progressed status (**Figure 4F**, **4G**). Through the integration of uni- and multivariate-Cox regression methods, a necroptosis gene signature independently predicted recurrence-free survival (**Figure 4H**, **4I**).

Biologic functions underlying the necroptosis prognostic model

Sister chromatid segregation, mitotic sister chromatid segregation, and chromosome condensation presented higher enrichment in high-risk prostatic carcinoma, with lower enrichment of cellular response to zinc ion, detoxification of copper ion, and stress response to metal ion (**Figure 5A**). In **Figure 5B**, cohesion complex, condensed nuclear chromosome kinetochore, and condensed nuclear chromosome, and centromeric region were highly enriched in

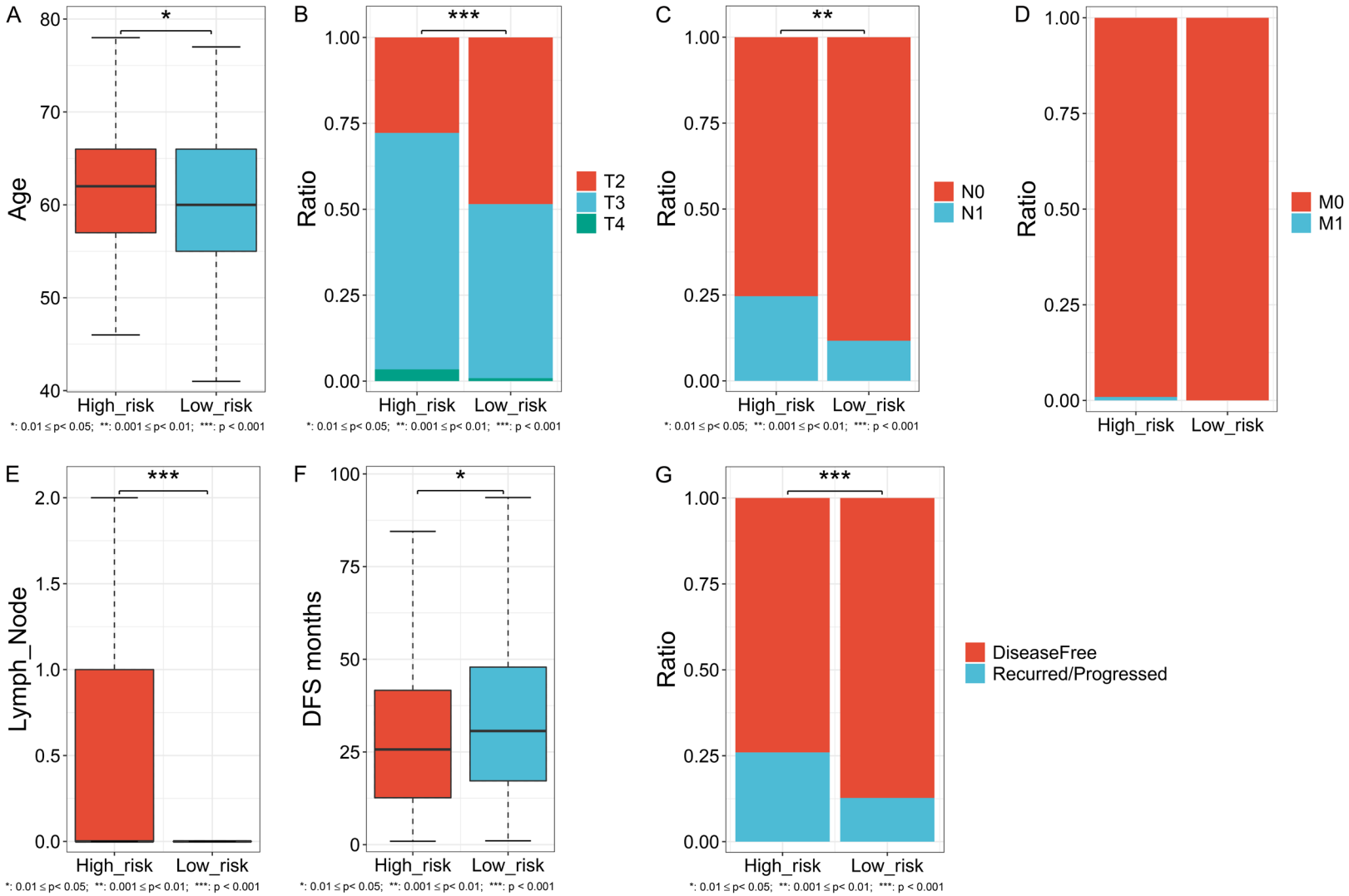
A
Age
High_risk
Low_risk
*: 0.01 ≤ p< 0.05; **: 0.001 ≤ p< 0.01; ***: p < 0.001
B
Ratio
T2
T3
T4
C
N0
N1
D
M0
M1
E
Lymph_Node
F
DFS months
G
DiseaseFree
Recurred/Progressed

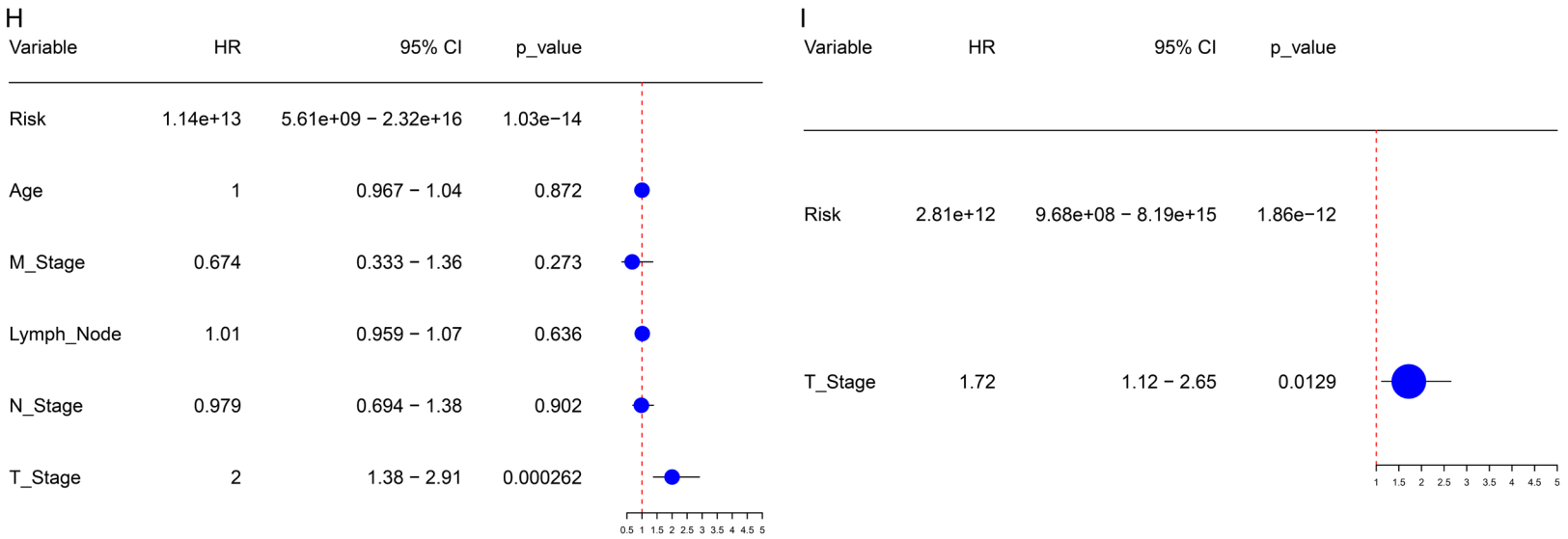

Figure 4. Clinical trait relevance of the necroptosis gene signature and its predictive independence. A-G. The heterogeneity in clinical data in low- and high-risk prostatic carcinoma. *P<0.05; **P<0.01; ***P<0.001. H, I. Uni- and multivariate-Cox regression results on the necroptosis gene signature and clinical variables with recurrence-free survival.

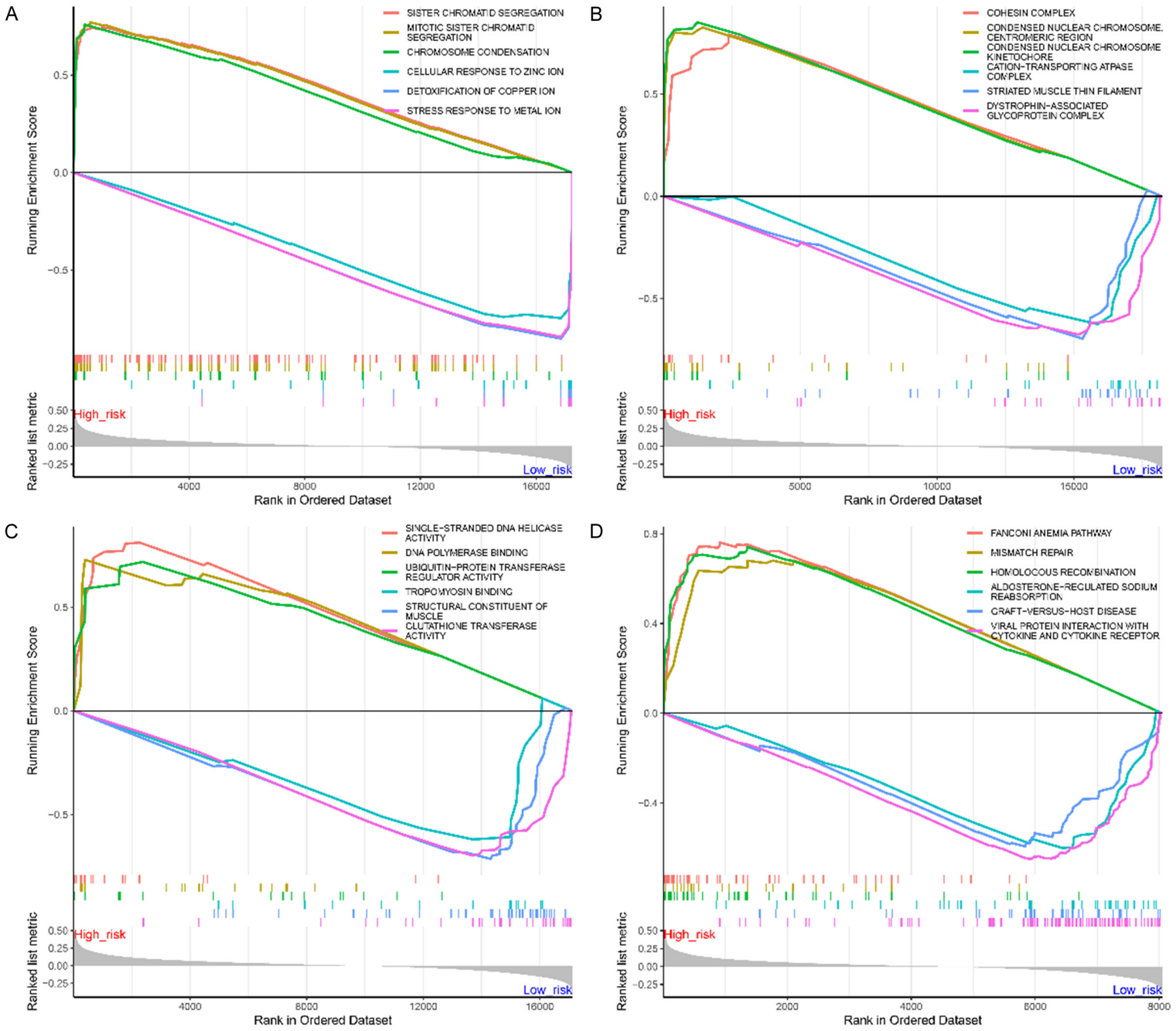
A
SISTER CHROMATID SEGREGATION
MITOTIC SISTER CHROMATID SEGREGATION
CHROMOSOME CONDENSATION
CELLULAR RESPONSE TO ZINC ION
DETOXIFICATION OF COPPER ION
STRESS RESPONSE TO METAL ION
Running Enrichment Score
Ranked list metric
High_risk
Low_risk
Rank in Ordered Dataset
B
COHESIN COMPLEX
CONDENSED NUCLEAR CHROMOSOME, CENTROMERIC REGION
CONDENSED NUCLEAR CHROMOSOME KINETOCHORE
CATION-TRANSPORTING ATPASE COMPLEX
STRIATED MUSCLE THIN FILAMENT
DYSTROPHIN-ASSOCIATED GLYCOPROTEIN COMPLEX
C
SINGLE-STRANDED DNA HELICASE ACTIVITY
DNA POLYMERASE BINDING
UBIQUITIN-PROTEIN TRANSFERASE REGULATOR ACTIVITY
TROPOMYOSIN BINDING
STRUCTURAL CONSTITUENT OF MUSCLE
GLUTATHIONE TRANSFERASE ACTIVITY
D
FANCONI ANEMIA PATHWAY
MISMATCH REPAIR
HOMOLOGOUS RECOMBINATION
ALDOSTERONE-REGULATED SODIUM REABSORPTION
GRAFT-VERSUS-HOST DISEASE
VIRAL PROTEIN INTERACTION WITH CYTOKINE AND CYTOKINE RECEPTOR

Figure 5. Biologic functions underlying the necroptosis prognostic model. (A-D) Gene set enrichment analysis (GSEA) illustrating the (A) biologic processes, (B) cellular components, and (C) molecular functions along with (D) Kyoto Encyclopedia of Genes and Genomes (KEGG) pathways with the enrichment variations between low- and high-risk prostatic carcinoma.

high-risk cases, with the lowly enriched striated muscle thin filaments, dystrophin-associated glycoprotein complex, and cation-transporting ATPase complex. Additionally, the higher enrichment of single-stranded DNA helicase activity, DNA polymerase binding, and ubiquitin-protein transferase regulator activity was investigated in high-risk specimens, with a lower enrichment of structural constituent of muscle, glutathione transferase activity, and tropomyosin binding (**Figure 5C**). Fanconi anemia pathway, homologous recombination, and mismatch repair presented a notable activation in high-risk specimens (**Figure 5D**). Meanwhile, the enrichment of viral protein interaction with cytokine and cytokine receptor, aldosterone-regulated sodium reabsorption, and graft-versus-host disease was investigated in low-risk cases.

Somatic mutation heterogeneity in low- versus high-risk prostatic carcinoma

Tumor mutational burden (TMB) exhibited a higher score in high- relative to low-risk specimens (**Figure 6A**, **6B**). Somatic mutation frequencies were investigated. Overall, the high-risk group occurred the higher mutation (**Figure 6C**, **6D**). Notably, TP53, BSN, APC, TRANK1, DNAH9, and SALL1 owned higher mutated frequencies in high-risk cases, with lower mutated frequencies of PDZRN3, and TRIO (**Figure 6E**). In addition, higher mutation co-occurrence was investigated in high- versus low-risk prostatic carcinoma (**Figure 6F**, **6G**).

Heterogeneous treatment responses in low- relative to high-risk patients

High-risk patients had a higher sensitivity to AZD2014, AZD5438, AZD6482, AZD8186, Entospletinib, ERK_2440, ERK_6604, GNE-317, IRAK4_4710, JAK1_8709, KU-55933, Obatoclax Mesylate, PD0325901, Sapitinib, SCH772984, Selumetinib, Trametinib, and WZ-4003, with a lower sensitivity to Sepantronium bromide, UMI-77, Vorinostat, and WIKI4 (**Figure 7A**, **7B**). Through considering the higher T-cell inflammation score (**Figure 7C**) as well as lower TIDE score (**Figure 7D**, **7E**), low-risk individuals had a higher chance to respond to immunotherapy.

Immune infiltration heterogeneity across low- and high-risk prostatic carcinoma

With CIBERSORT, we scored the infiltration of 22 immune cell compositions across prostatic carcinoma (**Figure 8A**). M2 and M1 macrophages possessed higher infiltration in high- versus low-risk prostatic carcinoma (**Figure 8B**, **8C**). In addition, a lower infiltration of activated dendritic cells, neutrophils, activated mast cells, monocytes, plasma cells, and CD4 memory resting T cells was found in the high-risk group. It was also noted that there were close relationships between immune cell compositions (**Figure 8D**).

Discussion

This work defined a necroptosis-based prognostic signature composed of BCL2, BCL2L11, BNIP3, CASP8, CYLD, HDAC9, IDH2, IPMK, MYC, PLK1, TNF, TNFRSF1A, and TSC1, that can effectively and independently predict recurrence of prostatic carcinoma patients, especially within one year. Also, high-risk individuals exhibited older age, more advanced T, N, M stage, shorter disease-free survival and more recurred/progressed status. Previously, Li et al. constructed a necroptosis-related prognostic model composed of ALOX15, BCL2, IFNA1, PYGL and TLR3 for prostatic adenocarcinoma patients [27].

Tumorigenic pathways (Fanconi anemia pathway, homologous recombination, and mismatch repair) presented increased activity in high-risk cases, thus potentially worsening prostate carcinoma survival. In addition, we observed that higher somatic mutations occurred in high-risk individuals, notably highly mutated TP53, BSN, APC, TRANK1, DNAH9, and SALL1.

Prostatic carcinoma is a heterogeneous malignancy, but the current treatment is not based upon molecular stratification. High-risk patients were sensitive to AZD2014, AZD5438,

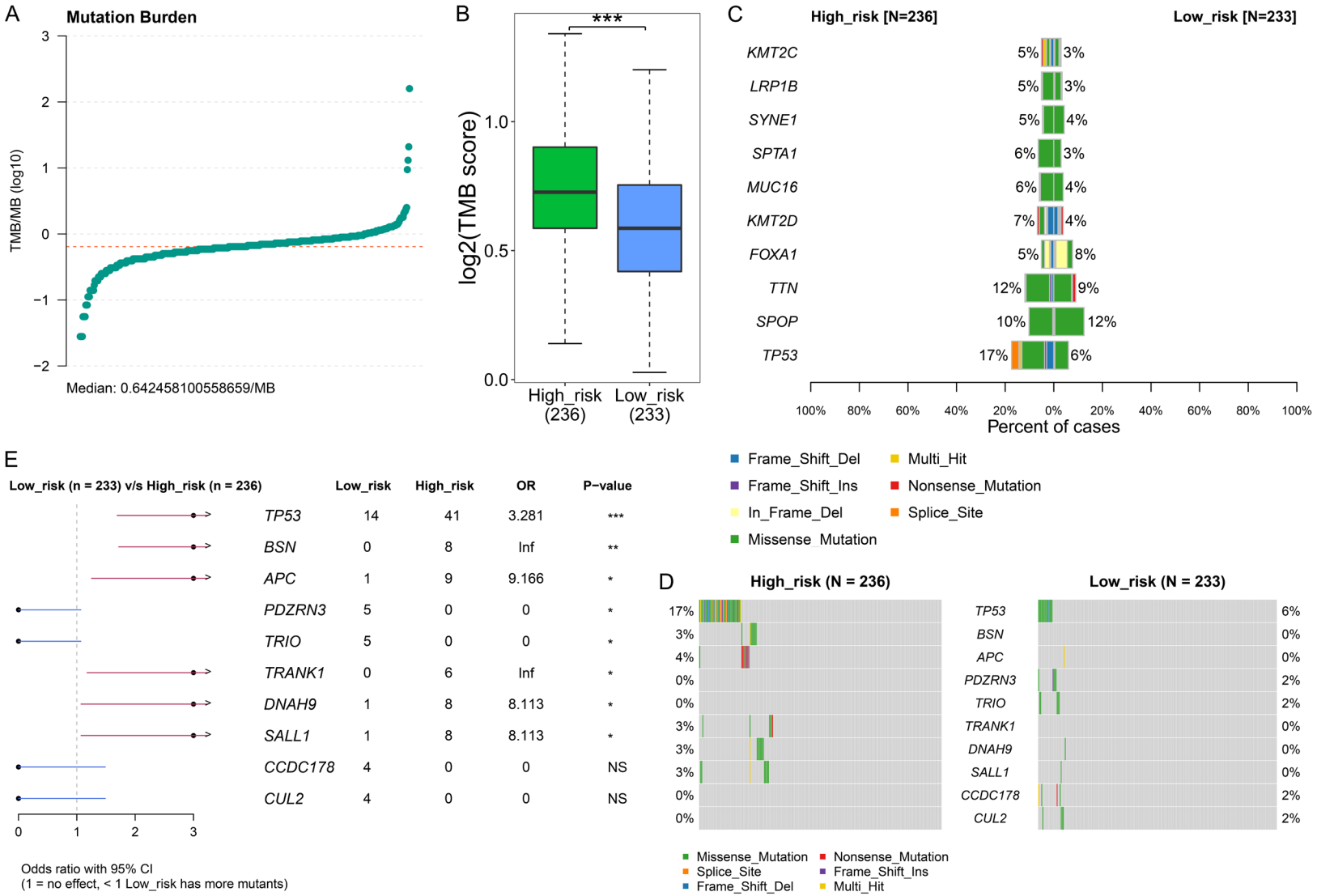
A
Mutation Burden
TMB/MB (log10)
Median: 0.642458100558659/MB
B
***
log2(TMB score)
High_risk (236)
Low_risk (233)
C
High_risk [N=236]
Low_risk [N=233]
KMT2C 5% 3%
LRP1B 5% 3%
SYNE1 5% 4%
SPTA1 6% 3%
MUC16 6% 4%
KMT2D 7% 4%
FOXA1 5% 8%
TTN 12% 9%
SPOP 10% 12%
TP53 17% 6%
Percent of cases
Frame_Shift_Del
Frame_Shift_Ins
In_Frame_Del
Missense_Mutation
Multi_Hit
Nonsense_Mutation
Splice_Site
E
Low_risk (n = 233) v/s High_risk (n = 236)
Low_risk High_risk OR P−value
TP53 14 41 3.281 ***
BSN 0 8 Inf **
APC 1 9 9.166 *
PDZRN3 5 0 0 *
TRIO 5 0 0 *
TRANK1 0 6 Inf *
DNAH9 1 8 8.113 *
SALL1 1 8 8.113 *
CCDC178 4 0 0 NS
CUL2 4 0 0 NS
Odds ratio with 95% CI
(1 = no effect, < 1 Low_risk has more mutants)
D
High_risk (N = 236)
Low_risk (N = 233)
TP53 17% 6%
BSN 3% 0%
APC 4% 0%
PDZRN3 0% 2%
TRIO 0% 2%
TRANK1 3% 0%
DNAH9 3% 0%
SALL1 3% 0%
CCDC178 0% 2%
CUL2 0% 2%
Missense_Mutation
Nonsense_Mutation
Splice_Site
Frame_Shift_Ins
Frame_Shift_Del
Multi_Hit

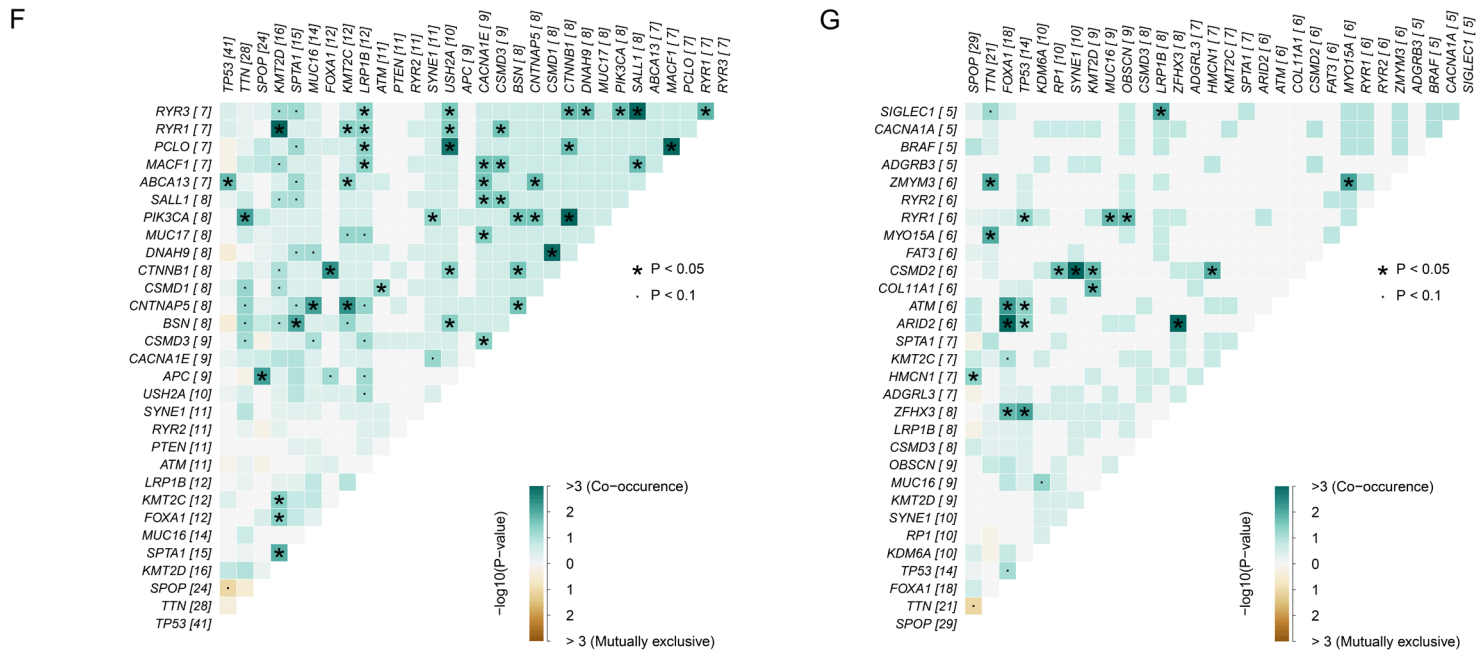

Figure 6. Somatic mutation heterogeneity in low- versus high-risk prostatic carcinoma. (A) Tumor mutational burden (TMB) distribution across prostatic carcinoma specimens. (B) Comparing TMB score in low- relative to high-risk cases. (C, D) Somatic mutation frequencies and classifications in the two groups. (E) Comparing the frequencies of mutated genes between groups. (F, G) Co-occurrence and mutual exclusion of mutated genes in (F) high- and (G) low-risk specimens. *P<0.05; **P<0.01; ***P<0.001; ns: P>0.05.

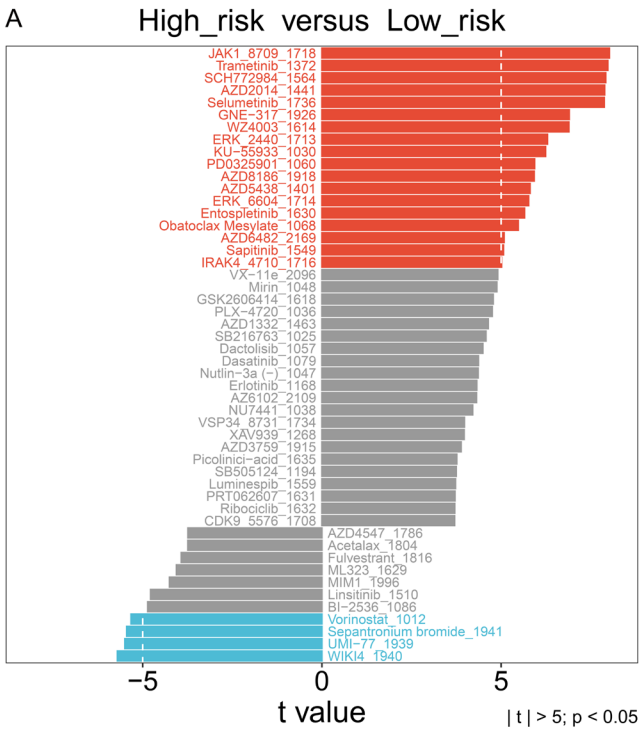
A
High_risk versus Low_risk
JAK1_8709_1718
Trametinib_1372
SCH772984_1564
AZD2014_1441
Selumetinib_1736
GNE−317_1926
WZ4003_1614
ERK_2440_1713
KU−55933_1030
PD0325901_1060
AZD8186_1918
AZD5438_1401
ERK_6604_1714
Entospletinib_1630
Obatoclax Mesylate_1068
AZD6482_2169
Sapitinib_1549
IRAK4_4710_1716
VX−11e_2096
Mirin_1048
GSK2606414_1618
PLX−4720_1036
AZD1332_1463
SB216763_1025
Dactolisib_1057
Dasatinib_1079
Nutlin−3a (−)_1047
Erlotinib_1168
AZ6102_2109
NU7441_1038
VSP34_8731_1734
XAV939_1268
AZD3759_1915
Picolinici−acid_1635
SB505124_1194
Luminespib_1559
PRT062607_1631
Ribociclib_1632
CDK9_5576_1708
AZD4547_1786
Acetalax_1804
Fulvestrant_1816
ML323_1629
MIM1_1996
Linsitinib_1510
BI−2536_1086
Vorinostat_1012
Sepantronium bromide_1941
UMI−77_1939
WIKI4_1940
−5
0
5
t value
| t | > 5; p < 0.05

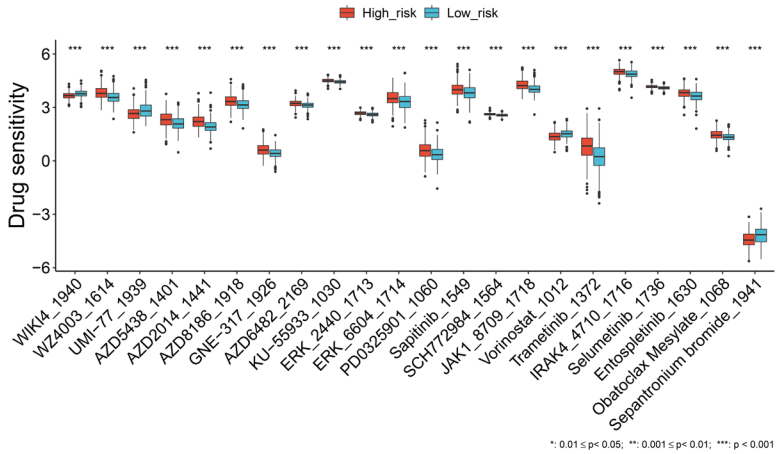
B
High_risk
Low_risk
Drug sensitivity
6
3
0
−3
−6
WIKI4_1940
WZ4003_1614
UMI−77_1939
AZD5438_1401
AZD2014_1441
AZD8186_1918
GNE−317_1926
AZD6482_2169
KU−55933_1030
ERK_2440_1713
ERK_6604_1714
PD0325901_1060
Sapitinib_1549
SCH772984_1564
JAK1_8709_1718
Vorinostat_1012
Trametinib_1372
IRAK4_4710_1716
Selumetinib_1736
Entospletinib_1630
Obatoclax Mesylate_1068
Sepantronium bromide_1941
*: 0.01 ≤ p< 0.05; **: 0.001 ≤ p< 0.01; ***: p < 0.001

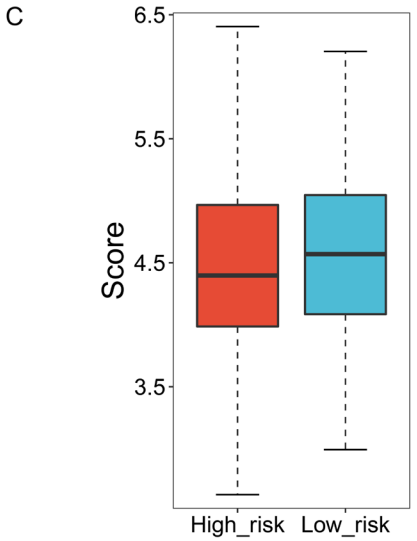
C
Score
6.5
5.5
4.5
3.5
High_risk
Low_risk

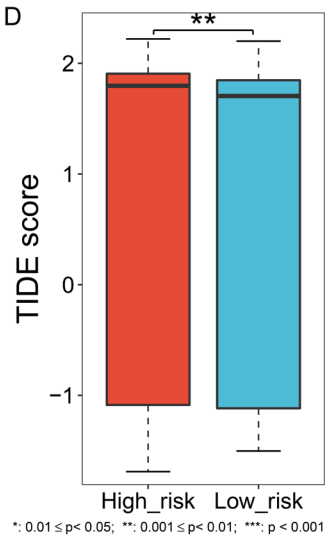
D
**
TIDE score
2
1
0
−1
High_risk
Low_risk
*: 0.01 ≤ p< 0.05; **: 0.001 ≤ p< 0.01; ***: p < 0.001

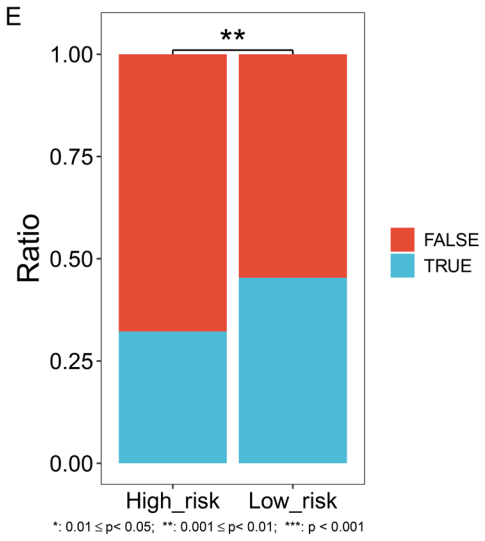
E
**
Ratio
1.00
0.75
0.50
0.25
0.00
FALSE
TRUE
High_risk
Low_risk
*: 0.01 ≤ p< 0.05; **: 0.001 ≤ p< 0.01; ***: p < 0.001

Figure 7. Heterogeneous treatment responses in low- relative to high-risk patients. A. Differences in drug sensitivity in high- versus low-risk prostatic carcinoma. B. Comparing the drug responses between groups. C. T-cell inflamed score across low- or high-risk cases. D. Tumor Immune Dysfunction and Exclusion (TIDE) score difference between groups. E. The ratios of immunotherapy responders in the two groups. $^{**}P<0.01$; $^{***}P<0.001$.

AZD6482, AZD8186, Entospletinib, ERK_2440, ERK_6604, GNE-317, IRAK4_4710, JAK1_8709, KU-55933, Obatoclax Mesylate, PD0325901, Sapitinib, SCH772984, Selumetinib, Trametinib, and WZ4003. In addition, those with low risk exhibited increased sensitivity to Sepantronium bromide, UMI-77, Vorinostat, and WIKI4. Prior research has demonstrated the anti-prostatic carcinoma properties of most compounds. AZD2014, a mTORC1/2 dual inhibitor, exerts a potent antitumor function in docetaxel-sensitive and -resistant castration-resistant prostate carcinoma [30]. Suppression of PI3Kβ pathway by AZD8186 mitigates growth of PTEN-deficient prostatic carcinoma solely or combined with docetaxel [31]. A phase I cohort showed that AZD8186 monotherapy, a selective PI3Kβ inhibitor, has antitumor activity in advanced solid tumors [32]. KU-55933, an ATM inhibitor, triggers apoptosis and mitigates motility through blocking GLUT1-induced glucose uptake in aggressive malignant cells [33]. Sepantronium bromide, a small molecule survivin suppressant, has time-dependent antitumor activity [34]. Vorinostat in combination with bortezomib synergistically result in ubiquitinated protein accumulation in prostatic carcinoma [35]. Vorinostat combined with DACA exhibit antitumor activity against hormone-refractory metastatic prostate carcinoma by dually mitigating histone deacetylase and topoisomerase I [36]. Prostatic carcinoma is immunologically “cold” and mostly has resistance to immunotherapy owing to low tumor-infiltrating T cells [37]. Clinical trials have proven that Nivolumab in combination with Ipilimumab can effectively treat metastatic castration-resistant prostatic carcinoma [38]. Based upon higher T-cell inflamed score and lower TIDE score, low-risk individuals possibly responded to immunotherapy. The necroptosis-based gene signature we propose might assist to select appropriate immunotherapeutic options.

High-risk prostatic carcinoma patients exhibited increased infiltration of M2 and M1 macrophages, with reduced infiltration of activated dendritic cells, neutrophils, activated mast cells, monocytes, plasma cells, and CD4 memory resting T cells. M2 macrophages associate with tumor extension and metastases in localized and metastatic prostatic carcinoma [39], and facilitate angiogenesis through VEGF-dependent signaling [40]. Prior research unveils that M2 macrophages are capable of inferring with biochemical recurrence of localized prostatic carcinoma following radical prostatectomy [41]. Activated dendritic cells correlate with prolonged survival duration [42], and a phase I/II trial showed an excellent effect of dendritic cell-based immunotherapy for patients with rising prostate-specific antigen following primary prostatectomy or salvage radiotherapy [43]. A increased neutrophil-to-lymphocyte ratio correlates with shorter overall survival for metastatic patients who received chemotherapy or not [44]. Reduced intratumoral mast cells are in relation to an increased risk of prostatic carcinoma recurrence [45]. Black men die more usually from prostatic carcinoma, and an increased plasma cell infiltrate is linked with recurrence-free survival after surgical resection [46]. Combining prior research, the heterogeneous infiltration of immune cells contributed to the different recurrence outcomes of prostatic carcinoma.

Although previous studies have established several genetic signatures for prediction of prostatic carcinoma recurrence, as far as we know, there is still a lack of necroptosis-based signatures. Our study possibly fills that gap. However, the shortcomings of this study should be pointed out. First, although we proved the potential of a necroptosis-based prognostic model in recurrence prediction, prospective cohorts are required. Moreover, the role of the signature in prediction of immunotherapy response must be confirmed in immunotherapy cohorts.

Conclusion

Collectively, the necroptosis-based genetic signature comprising BCL2, BCL2L11, BNIP3, CASP8, CYLD, HDAC9, IDH2, IPMK, MYC, PLK1,

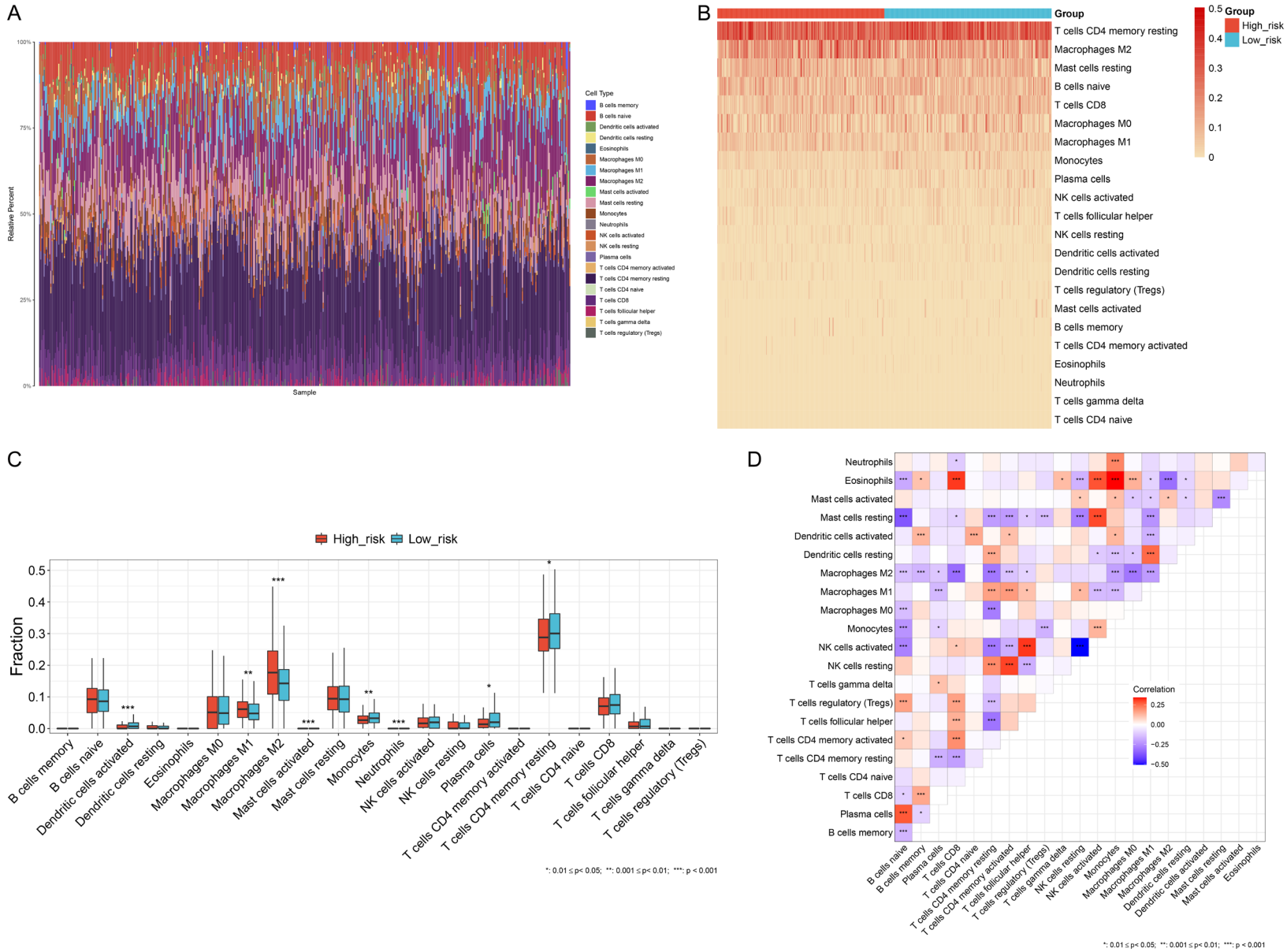

Figure 8. Immune infiltration heterogeneity across low- and high-risk prostatic carcinoma. A. Landscape of the abundance of immune cell components across prostatic carcinoma. B, C. Comparing the immune infiltration between low- and high-risk cases. D. Interactions between immune cell compositions. *P<0.05; **P<0.01; ***P<0.001.

TNF, TNFRSF1A, and TSC1 exhibited efficacy in prediction of prostatic carcinoma recurrence and treatment response. Despite this, its clinical feasibility must be verified in our future research.

Acknowledgements

This work was supported by grants from Jiangxi Youth Science Fundation (20161BAB215250), Youth Fundation of Second Affiliated Hospital of Nanchang University (2016YNQN12029), Jiangxi Provincial Health Fund for Traditional Chinese Medicine (2019A027), Jiangxi Health and Family Planning Commission Fundation (202130387, 2022A342), National Natural Science Foundation of China (81860455), The Natural Science Foundation of Jiangxi (2019-ACB20010).

Disclosure of conflict of interest

None.

Abbreviations

TCGA, the Cancer Genome Atlas; FC, fold change; GO, Gene Ontology; KEGG, Kyoto Encyclopedia of Genes and Genomes; LASSO, Least absolute shrinkage and selection operator; ROC, receiver operator characteristic curve; GSEA, Gene set enrichment analysis; TIDE, Tumor Immune Dysfunction and Exclusion; DFS, disease-free survival; TMB, tumor mutational burden.

Address correspondence to: Jun Luo, Department of Rehabilitation Medicine, The Second Affiliated Hospital of Nanchang University, Nanchang 330006, Jiangxi, China. E-mail: luojun1786@163.com; Tao Zeng, Deparment of Urology, The Second Affiliated Hospital of Nanchang University, Nanchang 330006, Jiangxi, China. E-mail: zengtaonanchang@163.com; Zhiqiang Luo and Lidong Wu, Department of Emergency, The Second Affiliated Hospital of Nanchang University, Nanchang 330006, Jiangxi, China. E-mail: house911cuddy@hotmail.com (ZQL); dongguawu89@163.com (LDW)

References

[1] Ashrafizadeh M, Paskeh MDA, Mirzaei S, Gholami MH, Zarrabi A, Hashemi F, Hushmandi K, Hashemi M, Nabavi N, Crea F, Ren J, Klionsky DJ, Kumar AP and Wang Y. Targeting autophagy in prostate cancer: preclinical and clinical evidence for therapeutic response. J Exp Clin Cancer Res 2022; 41: 105.

[2] Li W and Shen MM. Prostate cancer cell heterogeneity and plasticity: insights from studies of genetically-engineered mouse models. Semin Cancer Biol 2022; 82: 60-67.

[3] Mai CW, Chin KY, Foong LC, Pang KL, Yu B, Shu Y, Chen S, Cheong SK and Chua CW. Modeling prostate cancer: what does it take to build an ideal tumor model? Cancer Lett 2022; 543: 215794.

[4] Goel S, Bhatia V, Biswas T and Ateeq B. Epigenetic reprogramming during prostate cancer progression: a perspective from development. Semin Cancer Biol 2022; 83: 136-151.

[5] Vettenranta A, Murtola TJ, Raitanen J, Raittinen P, Talala K, Taari K, Stenman UH, Tammela TLJ and Auvinen A. Outcomes of screening for prostate cancer among men who use statins. JAMA Oncol 2022; 8: 61-68.

[6] Gillessen S, Armstrong A, Attard G, Beer TM, Beltran H, Bjartell A, Bossi A, Briganti A, Bristow RG, Bulbul M, Caffo O, Chi KN, Clarke CS, Clarke N, Davis ID, de Bono JS, Duran I, Eeles R, Efstathiou E, Efstathiou J, Ekeke ON, Evans CP, Fanti S, Feng FY, Fizazi K, Frydenberg M, George D, Gleave M, Halabi S, Heinrich D, Higano C, Hofman MS, Hussain M, James N, Jones R, Kanesvaran R, Khauli RB, Klotz L, Leibowitz R, Logothetis C, Maluf F, Millman R, Morgans AK, Morris MJ, Mottet N, Mrabti H, Murphy DG, Murthy V, Oh WK, Ost P, O'Sullivan JM, Padhani AR, Parker C, Poon DMC, Pritchard CC, Rabah DM, Rathkopf D, Reiter RE, Rubin M, Ryan CJ, Saad F, Sade JP, Sartor O, Scher HI, Shore N, Skoneczna I, Small E, Smith M, Soule H, Spratt DE, Sternberg CN, Suzuki H, Sweeney C, Sydes MR, Taplin ME, Tilki D, Tombal B, Türkeri L, Uemura H, Uemura H, van Oort I, Yamoah K, Ye D, Zapatero A and Omlin A. Management of patients with advanced prostate cancer: report from the Advanced Prostate Cancer Consensus Conference 2021. Eur Urol 2022; 82: 115-141.

[7] Zhang T, Yin C, Fedorov A, Qiao L, Bao H, Beknazarov N, Wang S, Gautam A, Williams RM, Crawford JC, Peri S, Studitsky V, Beg AA, Thomas PG, Walkley C, Xu Y, Poptsova M, Herbert A and Balachandran S. ADAR1 masks the cancer immunotherapeutic promise of ZBP1-driven necroptosis. Nature 2022; 606: 594-602.

[8] Niu X, Chen L, Li Y, Hu Z and He F. Ferroptosis, necroptosis, and pyroptosis in the tumor microenvironment: perspectives for immunotherapy of SCLC. Semin Cancer Biol 2022; 86: 273-285.

[9] Xie J, Chen L, Tang Q, Wei W, Cao Y, Wu C, Hang J, Zhang K, Shi J and Wang M. A necroptosis-related prognostic model of uveal melanoma

was constructed by single-cell sequencing analysis and weighted co-expression network analysis based on public databases. Front Immunol 2022; 13: 847624.
[10] Deeraksa A, Pan J, Sha Y, Liu XD, Eissa NT, Lin SH and Yu-Lee LY. Plk1 is upregulated in androgen-insensitive prostate cancer cells and its inhibition leads to necroptosis. Oncogene 2013; 32: 2973-2983.
[11] Wang KJ, Wang KY, Zhang HZ, Meng XY, Chen JF, Wang P, Jiang JH and Ma Q. Up-regulation of RIP3 alleviates prostate cancer progression by activation of RIP3/MLKL signaling pathway and induction of necroptosis. Front Oncol 2020; 10: 1720.
[12] Fu W, Li H, Fu H, Zhao S, Shi W, Sun M and Li Y. The SIRT3 and SIRT6 promote prostate cancer progression by inhibiting necroptosis-mediated innate immune response. J Immunol Res 2020; 2020: 8820355.
[13] Markowitsch SD, Juetter KM, Schupp P, Hauschulte K, Vakhrusheva O, Slade KS, Thomas A, Tsaur I, Cinatl J Jr, Michaelis M, Efferth T, Haferkamp A and Juengel E. Shikonin reduces growth of docetaxel-resistant prostate cancer cells mainly through necroptosis. Cancers (Basel) 2021; 13: 882.
[14] Gong Y, Fan Z, Luo G, Yang C, Huang Q, Fan K, Cheng H, Jin K, Ni Q, Yu X and Liu C. The role of necroptosis in cancer biology and therapy. Mol Cancer 2019; 18: 100.
[15] Robinson MD, McCarthy DJ and Smyth GK. edgeR: a Bioconductor package for differential expression analysis of digital gene expression data. Bioinformatics 2010; 26: 139-140.
[16] Jain S, Lyons CA, Walker SM, McQuaid S, Hynes SO, Mitchell DM, Pang B, Logan GE, McCavigan AM, O'Rourke D, McArt DG, McDade SS, Mills IG, Prise KM, Knight LA, Steele CJ, Medlow PW, Berge V, Katz B, Loblaw DA, Harkin DP, James JA, O'Sullivan JM, Kennedy RD and Waugh DJ. Validation of a metastatic assay using biopsies to improve risk stratification in patients with prostate cancer treated with radical radiation therapy. Ann Oncol 2018; 29: 215-222.
[17] Yu G, Wang LG, Han Y and He QY. clusterProfiler: an R package for comparing biological themes among gene clusters. OMICS 2012; 16: 284-287.
[18] Wang Z, Yao J, Dong T and Niu X. Definition of a novel cuproptosis-relevant lncRNA signature for uncovering distinct survival, genomic alterations, and treatment implications in lung adenocarcinoma. J Immunol Res 2022; 2022: 2756611.
[19] Subramanian A, Tamayo P, Mootha VK, Mukherjee S, Ebert BL, Gillette MA, Paulovich A, Pomeroy SL, Golub TR, Lander ES and Mesirov JP. Gene set enrichment analysis: a knowledge-based approach for interpreting genome-wide expression profiles. Proc Natl Acad Sci U S A 2005; 102: 15545-15550.
[20] Liberzon A, Birger C, Thorvaldsdóttir H, Ghandi M, Mesirov JP and Tamayo P. The Molecular Signatures Database (MSigDB) hallmark gene set collection. Cell Syst 2015; 1: 417-425.
[21] Mayakonda A, Lin DC, Assenov Y, Plass C and Koeffler HP. Maftools: efficient and comprehensive analysis of somatic variants in cancer. Genome Res 2018; 28: 1747-1756.
[22] Yang W, Soares J, Greninger P, Edelman EJ, Lightfoot H, Forbes S, Bindal N, Beare D, Smith JA, Thompson IR, Ramaswamy S, Futreal PA, Haber DA, Stratton MR, Benes C, McDermott U and Garnett MJ. Genomics of Drug Sensitivity in Cancer (GDSC): a resource for therapeutic biomarker discovery in cancer cells. Nucleic Acids Res 2013; 41: D955-961.
[23] Maeser D, Gruener RF and Huang RS. oncoPredict: an R package for predicting in vivo or cancer patient drug response and biomarkers from cell line screening data. Brief Bioinform 2021; 22: bbab260.
[24] Ott PA, Bang YJ, Piha-Paul SA, Razak ARA, Bennouna J, Soria JC, Rugo HS, Cohen RB, O'Neil BH, Mehnert JM, Lopez J, Doi T, van Brummelen EMJ, Cristescu R, Yang P, Emancipator K, Stein K, Ayers M, Joe AK and Lunceford JK. T-cell-inflamed gene-expression profile, programmed death ligand 1 expression, and tumor mutational burden predict efficacy in patients treated with pembrolizumab across 20 cancers: KEYNOTE-028. J Clin Oncol 2019; 37: 318-327.
[25] Jiang P, Gu S, Pan D, Fu J, Sahu A, Hu X, Li Z, Traugh N, Bu X, Li B, Liu J, Freeman GJ, Brown MA, Wucherpfennig KW and Liu XS. Signatures of T cell dysfunction and exclusion predict cancer immunotherapy response. Nat Med 2018; 24: 1550-1558.
[26] Newman AM, Liu CL, Green MR, Gentles AJ, Feng W, Xu Y, Hoang CD, Diehn M and Alizadeh AA. Robust enumeration of cell subsets from tissue expression profiles. Nat Methods 2015; 12: 453-457.
[27] Li XY, You JX, Zhang LY, Su LX and Yang XT. A novel model based on necroptosis-related genes for predicting prognosis of patients with prostate adenocarcinoma. Front Bioeng Biotechnol 2021; 9: 814813.
[28] Emelyanova M, Pudova E, Khomich D, Krasnov G, Popova A, Abramov I, Mikhailovich V, Filipenko M, Menshikova S, Tjulandin S and Pokataev I. Platinum-based chemotherapy for pancreatic cancer: impact of mutations in the homologous recombination repair and Fanco-

ni anemia genes. Ther Adv Med Oncol 2022; 14: 17588359221083050.
[29] Trigos AS, Pasam A, Banks P, Wallace R, Guo C, Keam S, Thorne H; kConFab, Mitchell C, Lade S, Clouston D, Hakansson A, Liu Y, Blyth B, Murphy D, Lawrentschuk N, Bolton D, Moon D, Darcy P, Haupt Y, Williams SG, Castro E, Olmos D, Goode D, Neeson P and Sandhu S. Tumor immune microenvironment of primary prostate cancer with and without germline mutations in homologous recombination repair genes. J Immunother Cancer 2022; 10: e003744.
[30] Li S, Sheng J, Liu Z, Fan Y, Zhang C, Lv T, Hu S, Jin J, Yu W and Song Y. Potent antitumour of the mTORC1/2 dual inhibitor AZD2014 in docetaxel-sensitive and docetaxel-resistant castration-resistant prostate cancer cells. J Cell Mol Med 2021; 25: 2436-2449.
[31] Hancox U, Cosulich S, Hanson L, Trigwell C, Lenaghan C, Ellston R, Dry H, Crafter C, Barlaam B, Fitzek M, Smith PD, Ogilvie D, D'Cruz C, Castriotta L, Wedge SR, Ward L, Powell S, Lawson M, Davies BR, Harrington EA, Foster E, Cumberbatch M, Green S and Barry ST. Inhibition of PI3Kβ signaling with AZD8186 inhibits growth of PTEN-deficient breast and prostate tumors alone and in combination with docetaxel. Mol Cancer Ther 2015; 14: 48-58.
[32] Choudhury AD, Higano CS, de Bono JS, Cook N, Rathkopf DE, Wisinski KB, Martin-Liberal J, Linch M, Heath EI, Baird RD, García-Carbacho J, Quintela-Fandino M, Barry ST, de Bruin EC, Colebrook S, Hawkins G, Klinowska T, Maroj B, Moorthy G, Mortimer PG, Moschetta M, Nikolaou M, Sainsbury L, Shapiro GI, Siu LL and Hansen AR. A phase I study investigating AZD8186, a potent and selective inhibitor of PI3Kβ/δ, in patients with advanced solid tumors. Clin Cancer Res 2022; 28: 2257-2269.
[33] Harris BRE, Zhang Y, Tao J, Shen R, Zhao X, Cleary MP, Wang T and Yang DQ. ATM inhibitor KU-55933 induces apoptosis and inhibits motility by blocking GLUT1-mediated glucose uptake in aggressive cancer cells with sustained activation of Akt. FASEB J 2021; 35: e21264.
[34] Kawano H, Shakushiro K, Nakata M, Kita A, Maeda A, Watanabe S, Sako K and Oku N. Antitumor efficacy and biodistribution of liposomal sepantronium bromide (YM155), a novel small-molecule survivin suppressant. Eur J Pharm Biopharm 2014; 88: 283-289.
[35] Sato A, Asano T, Ito K and Asano T. Vorinostat and bortezomib synergistically cause ubiquitinated protein accumulation in prostate cancer cells. J Urol 2012; 188: 2410-2418.
[36] Yu CC, Pan SL, Chao SW, Liu SP, Hsu JL, Yang YC, Li TK, Huang WJ and Guh JH. A novel small molecule hybrid of vorinostat and DACA displays anticancer activity against human hormone-refractory metastatic prostate cancer through dual inhibition of histone deacetylase and topoisomerase I. Biochem Pharmacol 2014; 90: 320-330.
[37] Morel KL, Sheahan AV, Burkhart DL, Baca SC, Boufaied N, Liu Y, Qiu X, Cañadas I, Roehle K, Heckler M, Calagua C, Ye H, Pantelidou C, Galbo P, Panja S, Mitrofanova A, Wilkinson S, Whitlock NC, Trostel SY, Hamid AA, Kibel AS, Barbie DA, Choudhury AD, Pomerantz MM, Sweeney CJ, Long HW, Einstein DJ, Shapiro GI, Dougan SK, Sowalsky AG, He HH, Freedman ML, Balk SP, Loda M, Labbé DP, Olson BM and Ellis L. EZH2 inhibition activates a dsRNA-STING-interferon stress axis that potentiates response to PD-1 checkpoint blockade in prostate cancer. Nat Cancer 2021; 2: 444-456.
[38] Sharma P, Pachynski RK, Narayan V, Fléchon A, Gravis G, Galsky MD, Mahammedi H, Patnaik A, Subudhi SK, Ciprotti M, Simsek B, Saci A, Hu Y, Han GC and Fizazi K. Nivolumab plus ipilimumab for metastatic castration-resistant prostate cancer: preliminary analysis of patients in the checkmate 650 trial. Cancer Cell 2020; 38: 489-499, e483.
[39] Lanciotti M, Masieri L, Raspollini MR, Minervini A, Mari A, Comito G, Giannoni E, Carini M, Chiarugi P and Serni S. The role of M1 and M2 macrophages in prostate cancer in relation to extracapsular tumor extension and biochemical recurrence after radical prostatectomy. Biomed Res Int 2014; 2014: 486798.
[40] Liang P, Henning SM, Grogan T, Elashoff D, Ye H, Cohen P and Aronson WJ. Effects of dietary omega-3 fatty acids on orthotopic prostate cancer progression, tumor associated macrophages, angiogenesis and T-cell activation-dependence on GPR120. Prostate Cancer Prostatic Dis 2022; 25: 539-546.
[41] Zhang Q, Xia J, Wang Y, Zhang J, Ji C, Cong R, Wang Y and Song N. Tumor infiltrating M2 macrophages could predict biochemical recurrence of localized prostate cancer after radical prostatectomy. Exp Cell Res 2019; 384: 111588.
[42] Vogelzang NJ, Beer TM, Gerritsen W, Oudard S, Wiechno P, Kukielka-Budny B, Samal V, Hajek J, Feyerabend S, Khoo V, Stenzl A, Csöszi T, Filipovic Z, Goncalves F, Prokhorov A, Cheung E, Hussain A, Sousa N, Bahl A, Hussain S, Fricke H, Kadlecova P, Scheiner T, Korolkiewicz RP, Bartunkova J and Spisek R; VIABLE Investigators. Efficacy and safety of autologous dendritic cell-based immunotherapy, docetaxel, and prednisone vs placebo in patients with metastatic castration-resistant prostate cancer: the VIABLE phase 3 randomized clinical trial. JAMA Oncol 2022; 8: 546-552.

[43] Fucikova J, Podrazil M, Jarolim L, Bilkova P, Hensler M, Becht E, Gasova Z, Klouckova J, Kayserova J, Horvath R, Fialova A, Vavrova K, Sochorova K, Rozkova D, Spisek R and Bartunkova J. Phase I/II trial of dendritic cell-based active cellular immunotherapy with DCVAC/PCa in patients with rising PSA after primary prostatectomy or salvage radiotherapy for the treatment of prostate cancer. Cancer Immunol Immunother 2018; 67: 89-100.

[44] Su S, Liu L, Li C, Zhang J and Li S. Prognostic role of pretreatment derived neutrophil to lymphocyte ratio in urological cancers: a systematic review and meta-analysis. Int J Surg 2019; 72: 146-153.

[45] Hempel HA, Cuka NS, Kulac I, Barber JR, Cornish TC, Platz EA, De Marzo AM and Sfanos KS. Low intratumoral mast cells are associated with a higher risk of prostate cancer recurrence. Prostate 2017; 77: 412-424.

[46] Weiner AB, Vidotto T, Liu Y, Mendes AA, Salles DC, Faisal FA, Murali S, McFarlane M, Imada EL, Zhao X, Li Z, Davicioni E, Marchionni L, Chinnaiyan AM, Freedland SJ, Spratt DE, Wu JD, Lotan TL and Schaeffer EM. Plasma cells are enriched in localized prostate cancer in Black men and are associated with improved outcomes. Nat Commun 2021; 12: 935.